



# Westerly jet stream controlled climate change mode since the Last Glacial Maximum in the northern Qinghai-Tibet Plateau

Yu Li\*, Simin Peng, Hebin Liu, Xinzhong Zhang, Wangting Ye, Qin Han, Yuxin Zhang, Lingmei Xu, Yichan Li

Key Laboratory of Western China's Environmental Systems (Ministry of Education), College of Earth and Environmental Sciences, Center for Hydrologic Cycle and Water Resources in Arid Region, Lanzhou University, Lanzhou, 730000, China

## ARTICLE INFO

### Article history:

Received 17 February 2020  
 Received in revised form 6 July 2020  
 Accepted 13 August 2020  
 Available online 26 August 2020  
 Editor: L. Robinson

### Keywords:

westerly jet stream  
 climate change mode  
 eolian sediments  
 climate simulations  
 Last Glacial Maximum

## ABSTRACT

Climate change from the northern Qinghai-Tibet Plateau (QTP) is affected by the combined effects of the Asian summer monsoon and the westerlies. However, changes in monsoon vapor transport and the westerly jet stream, as well as their effect to climate change mode there, are not clear at different time scales. Here we present composite research using paleoclimate reconstructions and ensemble simulations since the Last Glacial Maximum (LGM) on the basis of an eolian sedimentary sequence in the northern QTP. Results from 317 surface sediment samples show that pedogenic carbonate  $\delta^{18}\text{O}$  is affected both by precipitation and temperature, and organic carbon isotope ( $\delta^{13}\text{C}_{\text{org}}$ ) reflects the vegetation growth status in areas where precipitation is greater than 290 mm. Proxies from the sedimentary sequence and the Paleoclimate Modeling Intercomparison Project 3 (PMIP3) simulations show a close relationship between climate change mode in the northern QTP and the westerly jet stream whose movement is triggered by warm or cold conditions in the high-latitude regions. That is, when the climate is in cold/glacial period the westerly jet stream strengthens and moves southward, and the mountains become wetter. This climate change mode can be validated by records from mountains of North America and Africa. According to the CMIP5 simulations, the westerly jet stream will strengthen in the future, and climate in the northern QTP and the high-altitude region of the mid-latitudes will become wetter with global warming.

© 2020 Elsevier B.V. All rights reserved.

## 1. Introduction

Mid-latitude climates are commonly featured with vigorous circulation and are dominated by the two atmospheric systems, namely the polar air masses originating in high latitudes and maritime air masses stemming from the low latitudes (Fig. 1b-c, 2a) (Zhang and Lin, 1992; Wang, K. et al., 2005; Aguado and Burt, 2004; Barry et al., 2004). However, the impact of these changes on mid-latitude climate is still uncertain, in part due to the lack of long-term observational data (Overland et al., 2006). Global climate simulations have shown that the North Atlantic climate change and high latitude air masses have a crucial influence on the north-south migration of the westerly jet stream since the LGM (Kutzbach et al., 1993; COHMAP, 1988; Nagashima et al., 2011). The westerly jet stream was considered as a mechanism linking the high latitudes of the northern hemisphere with the climate of East Asia (Ding et al., 1998; Wu et al., 2008; An et al., 2012). By

contrast, the Asian summer monsoon is a low-latitude process that is related to the movement of the Intertropical Convergence Zone (ITCZ), which is fundamentally driven by orbital forcing and solar changes (An et al., 2012; Wang, Y. et al., 2005; Yancheva et al., 2007). Glacial forcing is also suggested to affect the Asian summer monsoon (especially EASM, e.g. Sun et al., 2015).

The interaction between the East Asian summer monsoon (EASM) and the westerly jet stream plays a significant role in East Asia climate changes over different time scales (Schiemann et al., 2009; Sampe and Xie, 2010; Chiang et al., 2015; Wang et al., 2017). Many studies have proven the impact of the location and intensity of the westerly jet stream on East Asian climate. In the timing of Holocene, the temporal variation in the position and orientation of the westerly jet stream determines the spatiotemporal precipitation pattern in China and Mongolia (Herzschuh et al., 2019). The differences in the transition timing and duration of the EASM seasonal stages during the Holocene, however, is in connection with the north-south displacement of westerlies relative to QTP (Kong et al., 2017). By interpreting the difference between Holocene  $\delta^{18}\text{O}$  records in the EASM and the synthesized Holocene

\* Corresponding author.

E-mail address: liyu@lzu.edu.cn (Y. Li).

average moisture index in arid central Asia as the distinction of two atmospheric systems, Chen et al. (2008, 2019) put forward the westerlies-dominated climatic regime. The highest-resolution drill core from Lake Qinghai logs the anti-correlated relationship of the EASM dominating the climate changes during the Holocene and westerly winds controlling the climate changes during the last glaciation (An et al., 2012). Furthermore, a synthesis, establishing a comprehensive database of precipitation  $\delta^{18}\text{O}$  over the QTP, suggests that recent precipitation  $\delta^{18}\text{O}$  over the northern TP is a result of the interaction between the westerlies and Indian monsoon (Yao et al., 2013). The latest research suggests that the meltwater from snow and glacier reconcile the westerlies and monsoon mode in Central Asia (Rao et al., 2019). From the foregoing, while many studies about the relationship between the EASM and the westerly jet stream are emerging, little information is available on the process and mechanism. In consequence, it is necessary to systematically clarify the dynamic mechanism on the long-term scale. Among them, the northeastern margin of the QTP is a core area for the synergistic effect of the monsoon and the westerly jet stream. In consequence, a better understanding of the relationship between different latitude driving mechanisms on the northeastern margin of the QTP will be of great significance for characterizing future variability in the mid-latitude hydroclimate.

Stable isotopes ( $\delta^{18}\text{O}$  and  $\delta^{13}\text{C}$ ) determined from various geological archives are widely used as indicators for changes of temperature, moisture condition, vegetation status and/or atmospheric circulation patterns in the past. The climate interpretation of the isotope results is a major challenge.  $\delta^{18}\text{O}$  records from polar ice cores indicate changes in temperature (Stuiver et al., 1995), but the ice core isotope records of the QTP show the effects of monsoon precipitation (Davis et al., 2005). Numerous studies suggest that the stalagmite  $\delta^{18}\text{O}$  in southern China reflects monsoon precipitation and can directly indicate the intensity of the East Asian summer monsoon (Wang, Y.Q. et al., 2005; Yuan et al., 2004; Dykoski et al., 2005; Cheng et al., 2009, 2016a,b). Compared to speleothem deposits,  $\delta^{18}\text{O}$  records in lacustrine carbonate sediments are often used to reflect the hydrological cycle and climate change (Deines, 1980; Farquhar et al., 1989). The measurement results of the isotope in the Jiuzhoutai loess profile indicate that changes of carbon and oxygen isotopes can better reflect climate change under continental climatic conditions (Zhang et al., 1990). Soil is an important carrier for studying modern processes. Some studies have shown that changes of pedogenic carbonate oxygen isotopic composition in soil are of environmental significance, and can be used to infer the evolution of surface vegetation types and precipitation, and to reconstruct past climate change (Cerling, 1984; Amundson et al., 1988; Huang et al., 2003; Wang and Liu, 2010). At present, there are few research results on the oxygen isotopic composition of soil carbonates in the northwestern region, and there is limited knowledge about its composition characteristics (Wang, K. et al., 2005). Because different photosynthesis pathways can lead to different distributions of organic carbon isotopes ( $\delta^{13}\text{C}_{\text{org}}$ ) between C3 and C4 plants (Wei and Gasse, 1999; Roberts et al., 2008),  $\delta^{13}\text{C}_{\text{org}}$  is commonly used as an organic geochemical proxy reflecting the primary productivity and vegetation type (Krishnamurthy et al., 1986; Meyers and Lallier-Vergès, 1999).  $\delta^{13}\text{C}_{\text{org}}$  of modern C3 plants ranges mainly from  $-34\text{‰}$  to  $-20\text{‰}$  with the most frequent values around  $-27\text{‰}$ , while values of modern C4 plants range principally from  $-19\text{‰}$  to  $-9\text{‰}$  with a mean value of approximately  $-13\text{‰}$  (Deines, 1980; Farquhar et al., 1989; O'Leary, 1988). According to previous studies, the  $\delta^{13}\text{C}_{\text{org}}$  value has a negative correlation with TOC, C/N ratio, and total pollen concentration which are mainly controlled by effective water (Li et al., 2014). As a result,  $\delta^{13}\text{C}_{\text{org}}$  is an ideal indicator of effective moisture change, and low  $\delta^{13}\text{C}_{\text{org}}$  values correspond to high available moisture (Li et al., 2016). Rao et al. (2017) and Zhang et al. (2019) investi-

gated the relationship between  $\delta^{13}\text{C}_{\text{org}}$  of surface soils and climatic factors (precipitation and temperature) to reconstruct the paleoclimate variations on regional and global scales. These results provide a basis for paleoclimate interpretation of various geological archives. Despite the complexities in explaining isotopic variations (He et al., 2016), the stable isotopes have considerable potential as proxies for regional climatic changes.

The Qilian section (QL), located in northern QTP, is an ideal site to study the competing influence of two atmospheric systems comprised of the EASM and the westerly jet stream on the northern QTP in the past (Fig. 2a). In this paper, we present a comprehensive analysis based on the combination of stable isotope reconstructions and ensemble simulations to explore the characteristics of the interaction between the EASM and the westerly jet stream. Our results show that the  $\delta^{18}\text{O}$  indicates the change of effective humidity, while  $\delta^{13}\text{C}_{\text{org}}$  reflects the regional vegetation growth status. Since the LGM, change in humidity represented by  $\delta^{18}\text{O}$  in the eolian sedimentary sequence is consistent with that of the mountains in the global westerlies, and the vegetation conditions reflected by  $\delta^{13}\text{C}_{\text{org}}$  have less fluctuation. A comparison with other paleoclimate records around the world reveals that this feature is widespread in high-altitude regions at mid-latitudes, such as North American and African mountain regions. Under an acceleration of the warming trend in the future (Brown and Caldeira, 2017), the further intensification of the westerly jet stream will significantly increase humidity in the northern QTP.

## 2. Regional setting

Located in the central hinterland of the Qilian Mountains, the study area is the largest marginal mountain system in the northern QTP. It has a unique climate mode which is affected by the interaction of the EASM and the westerly jet stream (Fig. 1b-c) (Schiemann et al., 2009; Sampe and Xie, 2010; Chiang et al., 2015; Wang et al., 2017). As a semi-arid area in northwest China, the study area is mainly covered by coniferous forests, shrubs and warm grasslands of the cold temperate zone. This is a typical highland continental climate with an average annual temperature of  $1^{\circ}\text{C}$  and an annual average rainfall of 420 mm. The seasonality of precipitation in the mid-latitudes is different from other regions (Fig. 1a). According to modern climatology researches, the sampling area is a sensitive region of climate change in China, which is mainly affected by the westerly jet stream and less benefited by the EASM water vapor transport in summer (Zhao, 1983; Li et al., 2012). As shown in Fig. 1b-c, the Asian monsoon water vapor will reach the northern QTP in summer while the westerly climate model dominates in winter. Therefore, the location of the sampling sites enables the eolian sedimentary sequence to record the effects of climate drivers. The QL ( $38^{\circ}9'31''\text{N}$ ,  $100^{\circ}16'12''\text{E}$ ) is at the Qilian County, Haibei Tibetan autonomous prefecture, Qinghai province in northwestern China.

## 3. Materials and methods

### 3.1. Sediment sampling

With the altitude of 2810 m a.s.l and a depth of 4 m (Fig. 2b). QL was sampled at 2 cm in interval, and a total of 200 eolian sedimentary samples were obtained for analysis of proxies. At an altitude range of 1100–4100 m, 317 surface sedimentary samples were collected along the Qilian Mountains ( $30^{\circ}01'\text{N}$ – $40^{\circ}03'\text{N}$ ,  $94^{\circ}03'\text{E}$ – $103^{\circ}05'\text{E}$ ) with a grid resolution of  $\sim 0.1^{\circ}$ . Fig. 2a indicates the sampling sites for all the surface samples. The sampling sites we selected were as far away as possible from the residential areas,

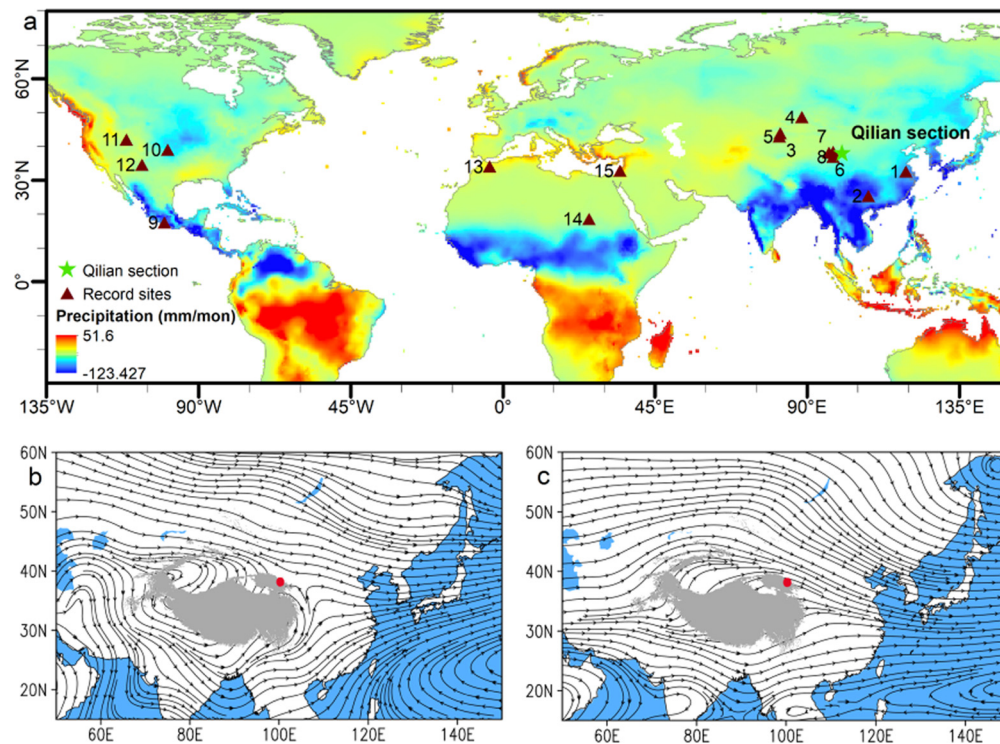


**Fig. 1.** Locations and circulations of the study area. **a** Locations of the Qilian eolian sedimentary sequence (green pentagon), distribution of paleoclimate records used in this study (red triangle), and the difference between winter (DJF) and summer (JJA) precipitation in 1969–2018 (shade). **b–c** Averaged atmospheric flow fields at 700 hPa isobaric in summer (JJA) and winter (DJF) from 1969–2018, respectively. (For interpretation of the colors in the figure(s), the reader is referred to the web version of this article.)

less affected by modern human activities, reflecting original vegetation and landscape.

### 3.2. AMS<sup>14</sup>C dating and isotope experimenting

Bulk organic matter was selected for AMS <sup>14</sup>C radiocarbon dating to establish chronologies for the QL. From the 4 m aeolian sedimentary sequence, 37 samples were selected at an average interval of about 10 cm for dating. The samples were pre-processed in the pretreatment laboratory of Lanzhou University, including sampling, sorting, drying. The AMS <sup>14</sup>C dates were measured at the Dating Laboratory of Peking University. The calibration of <sup>14</sup>C dates was performed using the OxCal v4.2.4 (Ramsey and Lee, 2013); r: 5; IntCal13 atmospheric curve (Reimer et al., 2013). The results are shown in Table 1. It may be due to the influence of redeposition that the chronological results at sections 134 cm, 144 cm, 154 cm, 164 cm, and 174 cm are older than the real ages. Thus, in the establishment of the age-depth model, the old ages of the above five samples were discarded. The relationship between age and depth can be drawn by a quadratic curve fitting ( $R^2 = 0.956$ ) at the QL (Fig. 2c).

By selecting a sample at each interval, 159 surface sedimentary samples and 100 eolian sedimentary samples were selected for carbon and oxygen isotope testing. Before the test, we dried and ground the samples in the pretreatment laboratory of Lanzhou University. Pedogenic carbonate  $\delta^{18}\text{O}$  values were measured on GasBenchII-MAT 253plus Mass Spectrometer from Beijing Createch Testing Technology Co., Ltd. The analytical precision for pedogenic carbonate  $\delta^{18}\text{O}$  values was 0.1‰. The instrument for the measurement of organic carbon isotope ( $\delta^{13}\text{C}_{\text{org}}$ ) is MAT 253plus, Flash EA elemental analyzer and ConFlo IV multi-purpose interface. The analytical accuracy of the  $\delta^{13}\text{C}_{\text{org}}$  can reach 0.2‰. Analysis and testing were done by Beijing Createch Testing Technology Co., Ltd. The carbon and oxygen isotope dataset of surface sediment in Qilian Mountains is shown in Table S1.

### 3.3. Modern observation data and paleoclimatic records

On the basis of a Climatic Research Unit (CRU) updated gridded climate dataset from the University of East Anglia, the monthly high-resolution ( $0.5^\circ \times 0.5^\circ$ ) land precipitation data (referred to as CRU TS4.01) are selected from 1969–2018 (Harris et al., 2013). Climatic Research Unit (CRU) monthly climate archives are obtained from the auspices of the World Meteorological Organization (WMO) in league with the US National Oceanographic and Atmospheric Administration (NOAA, via its National Climatic Data Center, NCDC). Simultaneously, the modern datasets including monthly zonal wind and meridional wind from 1969–2018 come through the National Centers for Environmental Prediction/National Center for Atmospheric Research (NCEP/NCAR) Global Reanalysis dataset (Kalnay et al., 1996). Along with 17 pressure levels 1000 to 10 hPa of zonal wind and meridional wind, the horizontal resolution is  $2.5^\circ \times 2.5^\circ$ . The China Meteorological Forcing Dataset was produced by merging a variety of data sources. This dataset currently covers the period 1979–2010 and can be obtained at <http://westdc.westgis.ac.cn/data/7a35329c-c53f-4267-aa07-e0037d913a21>. Its spatial resolution is  $0.1^\circ$  and its temporal resolution is 3-hr. In this paper, the mean annual temperature (MAT) and precipitation amount (MAP) are mainly used to analyze the relationship between the stable isotopes of surface sediments and the climate elements.

Various LGM paleoclimatic records have been collected throughout the world to reconstruct long-term climate variability (Fig. 1a and Table 2). We primarily pay close attention to paleo-precipitation and temperature changes since the LGM. The  $\delta^{18}\text{O}$  is mainly selected to indicate the climate changes in the mid-latitude regions of the global, which is still controversial to explain it as a monsoon vapor or precipitation proxy. Thus, in this paper we have selected records based on three criteria: (1) The selected records must have reliable chronologies. (2) The record length should cover most of the LGM without documented depositional hiatuses. (3)

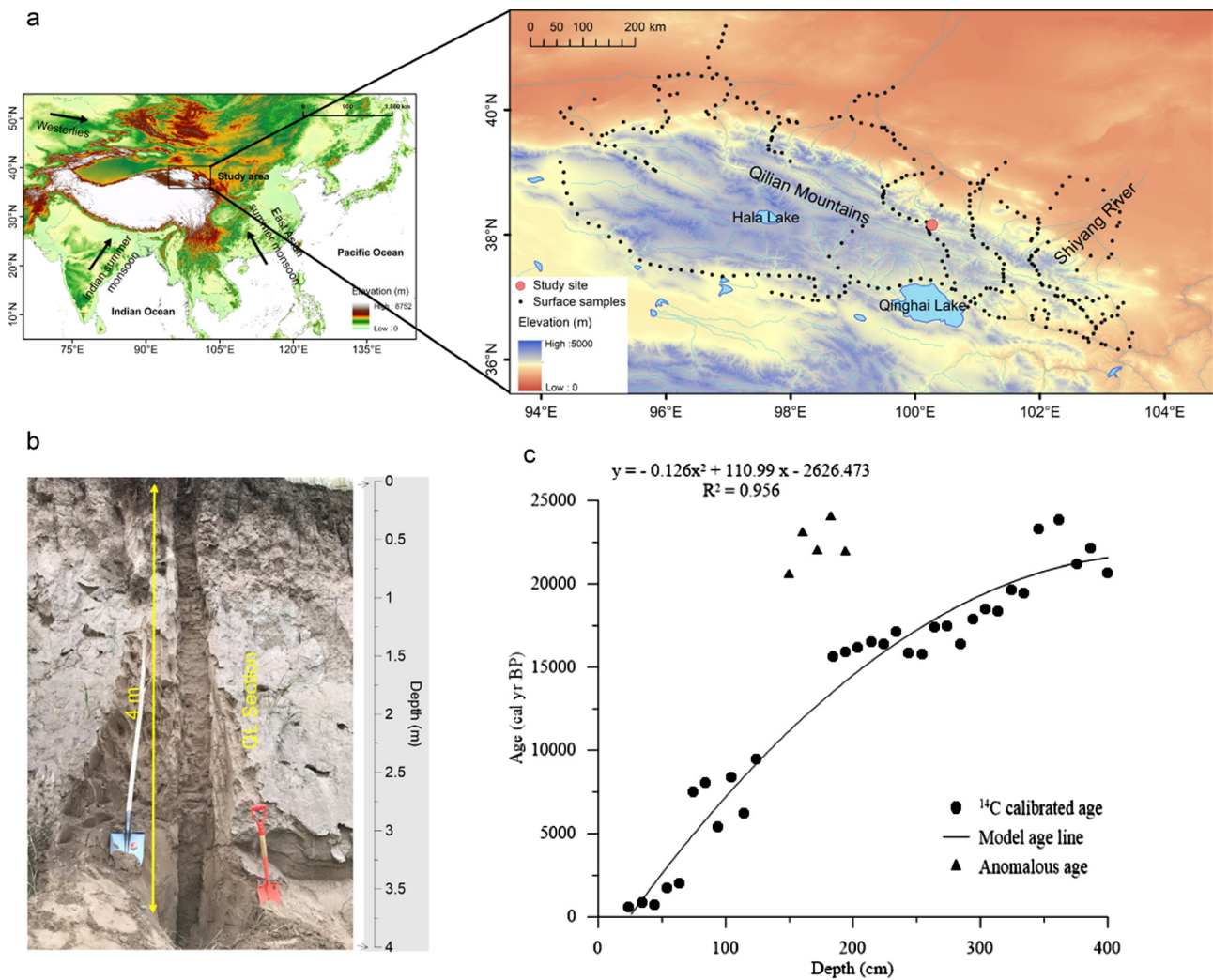


**Fig. 2.** Locations of the study area and distribution of surface sediments (a). Photo and chronological model of the Qilian section (b and c).

The proxies should indicate changes in precipitation or temperature. Following the above criteria, we collect fifteen records from various proxy data in the mid-latitude regions of the global since the LGM (Table 2 and Fig. 1a).

### 3.4. Paleoclimatic simulations and future projects

The Paleoclimate Modeling Intercomparison Project (PMIP) was launched in order to coordinate and encourage the systematic study of General Circulation Models (GCMs) and to understand the mechanisms of climate change and the role of climate feedbacks (Joussame et al., 1999). Thirty-seven coupled GCMs from the PMIP3 database were selected to analyze the mechanisms of climate change in this study (Table 3). The output data of the PMIP3 Last Glacial Maximum (LGM) and Mid-Holocene (MH) experiments are available at <https://esgf-node.llnl.gov/search/esgf-llnl/>. By chiefly interpolating various climate variables on the common  $1^\circ \times 1^\circ$  grid and then sorting the values of model simulations from minimum to maximum, we extracted the median value of all PMIP3 models used in this paper to evaluate the PMIP3 model simulations and acquire the scientific model simulation value. TraCE (Transient Climate Evolution) experiment from the National Center for Atmospheric Research, a state-of-art coupled ocean-atmosphere model, was chosen to calculate the LGM East Asian summer monsoon index (EASMI). The TraCE experiment is completed with the  $T31 \times 3$  resolution version of the Community Climate System

Model, version 3 (CCSM3) (Yeager et al., 2003; Liu et al., 2009; He, 2011). The atmospheric model has a horizontal resolution of  $\sim 3.75$  degrees and 26 vertical levels.

We chose the EASMI defined by Liu et al. (2014): the averaged summer meridional surface wind in East China ( $V850$  JJA,  $110^\circ\text{E}$ - $120^\circ\text{E}$ ;  $27^\circ\text{N}$ - $37^\circ\text{N}$ ) (Liu et al., 2014). The EASMI demonstrates the correspondence between the EASM monsoon winds and the precipitation  $\delta^{18}\text{O}$  values well, which resemble those of the Greenland temperature. Synchronously, the evolution of atmospheric water isotopes ( $\delta^{18}\text{O}_p$ ), defined as the precipitation weighted annual mean  $\delta^{18}\text{O}$  over China (average domain ( $100^\circ\text{E}$ - $115^\circ\text{E}$ ,  $27^\circ\text{N}$ - $36^\circ\text{N}$ )), was simulated by Liu et al. (2014) using the isotope-enabled atmospheric component model of the CCSM3 CAM3 (T31 resolution) (Liu et al., 2014). To detect the simulated EASMI at the fine horizontal resolution, the original data for the models were aggregated to the grid resolution of  $1^\circ \times 1^\circ$  using bilinear interpolation. Under the new greenhouse gas (GHG) emission scenarios termed "Representative Concentration Pathways" (RCPs), the CMIP5 set of experiments include simulations of 20th century climate (referred to as historical experiments, 1850 to 2005) and projection experiments (2006 to 2100) of 21st century climate (Moss et al., 2010; Taylor et al., 2012). The output databases from Thirty-one climate models were selected for the climate change projections in global under the RCP 8.5 scenario, which is a continuously rising radiative forcing pathway (Table 3). Aligned with PMIP3, all of the CMIP5 model data are interpolated by the cubic spline onto a com-

**Table 1**  
AMS <sup>14</sup>C ages for the Qilian section.

Laboratory number	Depth (cm)	Dating materials	<sup>14</sup> C age (yr BP)	Calibrated <sup>14</sup> C age (2σ) (cal.yr BP)
BA182070	334	Organic matter	16,075 ± 45	19,408 (19,229–19,569)
BA182071	324	Organic matter	16,260 ± 45	19,627 (19,473–19,838)
BA182072	314	Organic matter	15,110 ± 40	18,370 (18,191–18,529)
BA182073	304	Organic matter	15,205 ± 40	18,477 (18,338–18,609)
BA182074	294	Organic matter	14,665 ± 45	17,855 (17,679–18,010)
BA182075	284	Organic matter	13,605 ± 35	16,389 (16,215–16,594)
BA182076	274	Organic matter	14,330 ± 90	17,458 (17,148–17,721)
BA182077	264	Organic matter	14,275 ± 40	17,396 (17,193–17,562)
BA182078	254	Organic matter	13,130 ± 40	15,771 (15,584–15,975)
BA182079	244	Organic matter	13,190 ± 35	15,853 (15,696–16,025)
BA182080	234	Organic matter	14,080 ± 40	17,119 (16,933–17,363)
BA182081	224	Organic matter	13,580 ± 60	16,361 (16,155–16,614)
BA182082	214	Organic matter	13,685 ± 45	16,504 (16,295–16,760)
BA182083	204	Organic matter	13,450 ± 40	16,184 (16,005–16,354)
BA182084	194	Organic matter	13,215 ± 40	15,884 (15,720–16,059)
BA182085	184	Organic matter	13,055 ± 45	15,649 (15,379–15,850)
BA182086	174	Organic matter	16,225 ± 45	19,587 (19,425–19,786)
BA182087	164	Organic matter	17,740 ± 50	21,484 (21,250–21,725)
BA182088	154	Organic matter	16,290 ± 45	19,662 (19,503–19,874)
BA182089	144	Organic matter	17,090 ± 50	20,612 (20,440–20,807)
BA182090	134	Organic matter	15,100 ± 40	18,357 (18,171–18,512)
BA182091	124	Organic matter	8,420 ± 30	9,460 (9,334–9,337)
BA182092	114	Organic matter	5,410 ± 30	6,236 (6,129–6,139)
BA182093	104	Organic matter	7,575 ± 30	8,389 (8,350–8,417)
BA182094	94	Organic matter	4,695 ± 25	5,389 (5,321–5,420)
BA182095	84	Organic matter	7,250 ± 30	8,074 (8,001–8,163)
BA182096	74	Organic matter	6,615 ± 25	7,508 (7,443–7,449)
BA182097	64	Organic matter	2,055 ± 20	2,020 (1,948–2,066)
BA182098	54	Organic matter	1,810 ± 20	1,753 (1,640–1,643)
BA182099	44	Organic matter	845 ± 20	752 (701–790)
BA1820100	34	Organic matter	965 ± 20	856 (797–871)
BA1820101	24	Organic matter	660 ± 20	604 (561–595)
BA1820102	346	Organic matter	19,370 ± 60	23,324 (23,060–23,565)
BA1820103	362	Organic matter	19,790 ± 60	23,827 (20,933–21,420)
BA1820104	376	Organic matter	17,530 ± 60	21,176 (20,933–21,420)
BA1820105	386	Organic matter	18,280 ± 70	22,151 (21,907–22,365)
BA1820106	400	Organic matter	17,155 ± 50	20,689 (20,516–20,886)

**Table 2**  
Locations and sediment types of different study sites in the mid-latitude region that are referenced in the text (see Fig. 1a for site locations).

Code	Section	Latitude	Longitude	Elevation (m)	Dating method	Sediment type	Indicator	References
1	Hulu Cave	32.5	119.167	100 m	U-Th	Stalagmite	δ <sup>18</sup> O	Wang et al., 2001
2	Dongge Cave	25.283	108.083	680 m	U-Th	Stalagmite	δ <sup>18</sup> O	Yuan et al., 2004
3	Yili Valley	43.857	81.965	928 m	AMS <sup>14</sup> C	Lacustrine sediment	pollen	Li et al., 2011
4	Hoton-Nur	48.621	88.345	2083 m	AMS <sup>14</sup> C	Lake sediment	pollen	Rudaya et al., 2009
5	Kesang Cave	42.866	81.75	2000 m	U-Th	Stalagmite	δ <sup>18</sup> O	Cheng et al., 2016a, 2016b
6	Dunde Ice core	38.1	96.4	5325 m	AMS <sup>14</sup> C	Ice core	δ <sup>18</sup> O	Yao and Thompson, 1992
7	Hala Lake	38.3	97.583	4078 m	AMS <sup>14</sup> C	Lake sediment	δ <sup>18</sup> O	Yan and Wünnemann, 2014
8	Qinghai Lake	36.883	97.583	3200 m	AMS <sup>14</sup> C	Lake sediment	δ <sup>18</sup> O	Liu et al., 2007
9	Juxtaluca Cave	17.44	−100.083	750 m	U-Th	Stalagmite	δ <sup>18</sup> O	Lachniet et al., 2013
10	Lehman Caves	39.006	−99.16	2130 m	U-Th	Stalagmite	δ <sup>18</sup> O	Steponaitis et al., 2015
11	Bear Lake	42	−111.34	1805 m	AMS <sup>14</sup> C	Lake sediment	δ <sup>18</sup> O	Dean et al., 2006
12	Abo Arroyo	34.53	−106.78	1449 m	AMS <sup>14</sup> C	Lacustrine sediment	δ <sup>13</sup> C	Hall and Penner, 2013
13	Grotte de Piste	34	−4	1260 m	U-Th	Stalagmite	δ <sup>18</sup> O	Wassenburg et al., 2016
14	West Nubian Paleolake	18.5	25.5	556 m	AMS <sup>14</sup> C	Lacustrine sediment	δ <sup>18</sup> O	Abell and Hoelzmann, 2000
15	Levantine basin	32.74	34.65	892 m	AMS <sup>14</sup> C	Lacustrine sediment	Ba/Ca	Weldeab et al., 2014

mon 1° × 1° grid to calculate the median values under three times (2010s, 2011–2020; 2050s, 2051–2060; 2090s, 2091–2100).

## 4. Results

### 4.1. Surface and eolian sedimentary pedogenic carbonate δ<sup>18</sup>O and organic matter δ<sup>13</sup>C

As shown in Fig. 3a, the range of pedogenic carbonate δ<sup>18</sup>O, generally varying from −23.01‰ to −1.26‰, with an average value of −9.57‰. The most frequent pedogenic carbonate δ<sup>18</sup>O

values are around −8.5‰ to −5.5‰ (Fig. 3a). Fig. 3b–f shows the quadratic regression relationship between pedogenic carbonate δ<sup>18</sup>O values and altitudes, temperature and precipitation, respectively. No obvious relationship was found between pedogenic carbonate δ<sup>18</sup>O and altitude, but most of the negative values are in high altitudes. For further analysis, the 159 surface sedimentary pedogenic carbonate δ<sup>18</sup>O values were used for correlation analyses with the corresponding MAP and MAT (Fig. 3c–f). We found the positive relationship between both pedogenic carbonate δ<sup>18</sup>O and MAT ( $y = 0.29x - 10.41$ ,  $n = 159$ ,  $r^2 = 0.11$ ). Previous Holocene and modern lacustrine pedogenic carbonate δ<sup>18</sup>O stud-

**Table 3**  
Description of PMIP3-CMIP5 models used in this study.

Model name	Resolution	Last Glacial Maximum (LGM)	Mid-Holocene (MH)	Pre-Industrial (PI)	RCP8.5
ACCESS1-0	144×192	×	×	×	✓
ACCESS1-3	144×192	×	×	×	✓
bcc-csm1-1	64×128	×	✓	✓	×
CanESM2	64×128	×	×	×	✓
CCSM4	192×288	✓	✓	✓	✓
CMCC-CESM	48×96	×	×	×	✓
CMCC-CM	240×480	×	×	×	✓
CNRM-CM5	128×256	✓	✓	✓	✓
COSMOS-ASO	48×96	✓	×	✓	×
CSIRO-Mk3-6-0	96×192	×	✓	✓	✓
CSIRO-Mk3L-1-2	56×64	×	✓	✓	×
EC-EARTH-2-2	160×320	×	✓	×	×
FGOALS-g2	60×128	✓	✓	✓	×
FGOALS-s2	108×128	×	✓	✓	✓
GFDL-CM3	90×144	×	×	×	✓
GFDL-ESM2G	90×144	×	×	×	✓
GISS-E2-H	89×144	×	×	×	✓
GISS-E2-H-CC	89×144	×	×	×	✓
GISS-E2-R	89×144	✓	✓	✓	✓
GISS-E2-R-CC	89×144	×	×	×	✓
HadCM3	72×96	×	×	✓	×
HadGEM2-CC	144×192	×	✓	✓	✓
HadGEM2-ES	144×192	×	✓	✓	✓
inmcm4	120×180	×	×	×	✓
IPSL-CM5A-LR	96×96	✓	✓	✓	✓
IPSL-CM5A-MR	143×144	×	×	×	✓
IPSL-CM5B-LR	96×96	×	×	×	✓
MIROC5	128×256	×	×	×	✓
MIROC-ESM	64×128	✓	✓	✓	✓
MIROC-ESM-CHEM	64×128	×	×	×	✓
MPI-ESM-LR	96×192	×	×	×	✓
MPI-ESM-MR	96×192	×	×	×	✓
MPI-ESM-P	96×192	✓	✓	✓	×
MRI-CGCM3	160×320	✓	✓	✓	✓
MRI-ESM1	160×320	×	×	×	✓
NorESM1-M	96×144	×	×	×	✓
NorESM1-ME	96×144	×	×	×	✓

ies have demonstrated the temperature and evaporation effects in arid Asia (Yu et al., 2009; Zhang et al., 2011). Therefore, temperature has a certain effect on carbonate  $\delta^{18}\text{O}$  in the northern QTP. The relationship between pedogenic carbonate  $\delta^{18}\text{O}$  and precipitation is more special. With the change of precipitation, pedogenic carbonate  $\delta^{18}\text{O}$  is distributed in the shape of a mass, and is divided into two large masses with a boundary of 290 mm of precipitation (Fig. 3d). Pedogenic carbonate  $\delta^{18}\text{O}$  values less than 290 mm have less fluctuations and are irrelevant to MAP ( $y = -0.0005x - 8.48$ ,  $n = 74$ ,  $r^2 = 0.0001$ ) (Fig. 3e), while pedogenic carbonate  $\delta^{18}\text{O}$  values greater than 290 mm are significantly inversely related to MAP ( $y = -0.05x - 7.91$ ,  $n = 85$ ,  $r^2 = 0.36$ ) (Fig. 3f).

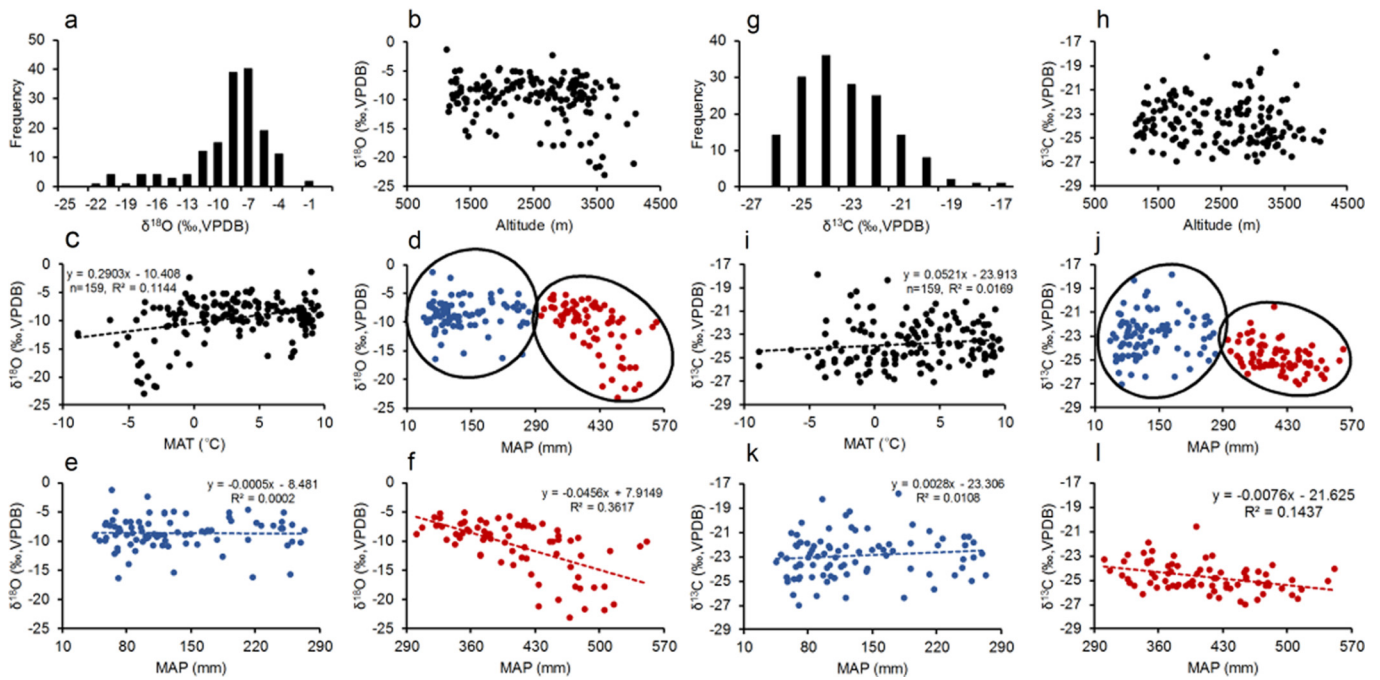
The integrated 159 values organic carbon isotope ( $\delta^{13}\text{C}_{\text{org}}$ ) (‰) scatter between  $-26.98\text{‰}$  and  $-17.83\text{‰}$ , with an average value of  $-23.76\text{‰}$  (Fig. 3g). The most frequent  $\delta^{13}\text{C}_{\text{org}}$  values are around  $-25\text{‰}$  to  $-23\text{‰}$  (Fig. 3g). The  $\delta^{13}\text{C}_{\text{org}}$  values were mostly within the range of those for C3 plants. This result indicates that the stable carbon composition of surface sediments in the northern QTP is mainly determined by C3 plants. Fig. 3h-l shows the quadratic regression relationship between surface sedimentary  $\delta^{13}\text{C}_{\text{org}}$  values and altitudes, temperature and precipitation, respectively. We can find an insignificant relationship between  $\delta^{13}\text{C}_{\text{org}}$  values and altitudes. For further analysis, the correlation analysis results of  $\delta^{13}\text{C}_{\text{org}}$  values and MAT and MAP are illustrated in Fig. 3i-l. There are insignificant negative relationships between  $\delta^{13}\text{C}_{\text{org}}$  and MAT ( $y = -0.05x - 23.91$ ,  $n = 159$ ,  $r^2 = 0.02$ ), which indicates that  $\delta^{13}\text{C}_{\text{org}}$  values are less sensitive to temperature. Similarly,  $\delta^{13}\text{C}_{\text{org}}$  is divided into two large masses with a boundary of 290 mm of

precipitation (Fig. 3j).  $\delta^{13}\text{C}_{\text{org}}$  values less than 290 mm have an insignificant positive correlation with MAP ( $y = -0.0028x - 23.31$ ,  $n = 74$ ,  $r^2 = 0.01$ ) (Fig. 3e), while  $\delta^{13}\text{C}_{\text{org}}$  values greater than 290 mm are significantly inversely related to MAP ( $y = -0.0076x - 21.63$ ,  $n = 85$ ,  $r^2 = 0.14$ ) (Fig. 3f).

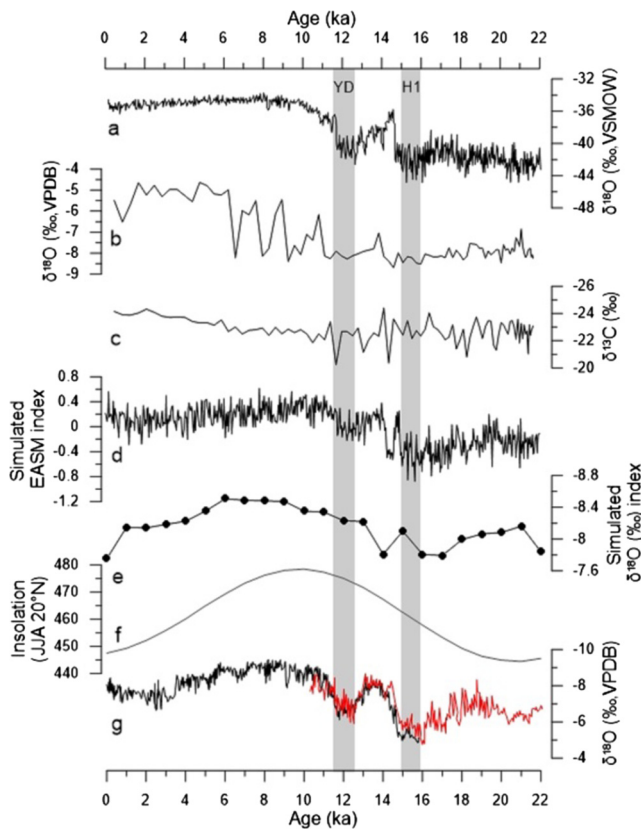
#### 4.2. Paleoclimate records and model simulations

Fig. 4 shows a comparison between the reconstructed climate variability using the stable isotopes and the simulated East Asian summer monsoon index (EASMI) and precipitation weighted summer  $\delta^{18}\text{O}$  using TRACE simulation since the LGM. They display a diverse changing trend between the mid-latitude climate and EASM. It is obvious that the simulated EASMI synchronously varies with precipitation weighted Chinese annual  $\delta^{18}\text{O}$  index in the snapshot simulations, which is consistent with EASM from Dongge Cave and Hulu Cave (Yuan et al., 2004; Wang et al., 2001). These evolutionary features state that the EASM is negatively correlated with the precipitation weighted Chinese annual  $\delta^{18}\text{O}$ , and the EASM intensity has changed less since the LGM.

During the last deglaciation, the EASM records and PMIP3 simulations suggest that the EASM was relatively weak, exhibiting no long-term change, which weakened the wind and made it difficult to transport water vapor to the inland. In addition, the distance from the northern QTP to the oceanic moisture source increased during the LGM, when the coastline moved southeastward by as much as 1000 km (An et al., 2012). Increased transport distance makes water vapor more difficult to reach the northern QTP. There-



**Fig. 3.** Results from surface sediment samples. **a-d** Frequency distribution of surface sedimentary pedogenic carbonate  $\delta^{18}\text{O}$  values and relationship between pedogenic carbonate  $\delta^{18}\text{O}$  and their altitudes, MAT and MAP. **e-f** The relationship between carbonate  $\delta^{18}\text{O}$  values less than 290 mm and MAP (**e**), and the relationship between carbonate  $\delta^{18}\text{O}$  values greater than 290 mm and MAP (**f**). **g-j** Frequency distribution of surface sedimentary  $\delta^{13}\text{C}_{\text{Org}}$  values and relationship between  $\delta^{13}\text{C}_{\text{Org}}$  values and their altitudes, MAT and MAP. **k-l** The relationship between  $\delta^{13}\text{C}_{\text{Org}}$  values less than 290 mm and MAP (**k**), and the relationship between  $\delta^{13}\text{C}_{\text{Org}}$  values greater than 290 mm and MAP (**l**).



**Fig. 4.** A comparison of the proxies and simulated indices. **a** NGRIP  $\delta^{18}\text{O}$  (Rasmussen et al., 2006). **b** The carbonate  $\delta^{18}\text{O}$  from QL (this study). **c**  $\delta^{13}\text{C}_{\text{Org}}$  values (this study). **d** Precipitation weighted Chinese annual  $\delta^{18}\text{O}$  index in the snapshot simulations (Liu et al., 2014). **e** The simulated EASMI since the LGM from TRACE model (Liu et al., 2014). **f** The LGM summer insolation at 20°N (Berger, 1978). **g** Cave speleothem  $\delta^{18}\text{O}$  values records from Dongge Cave and Hulu Cave (Yuan et al., 2004; Wang et al., 2001).

fore, we suggest that the monsoon rarely penetrated northwest to reach the northeastern QTP that is affected by modern monsoon water vapor in summer. During the Holocene, both the amplitude and variability of the EASM increased obviously, especially in the early Holocene. However, since the LGM, the reconstructed high-altitude carbonate  $\delta^{18}\text{O}$  values in the northeastern QTP has an increasing trend, which is opposite to the EASM variation, but similar to the NGRIP  $\delta^{18}\text{O}$  record that is closely correlated with warm or cold status in high-latitudes. It shows that carbonate  $\delta^{18}\text{O}$  values in mountainous areas is not controlled by monsoon vapor. Paleoclimate records from the interaction zone between the monsoon and the westerly jet stream in the mid-latitudes, as well as temperature proxies in the high-altitude region and moisture proxies in the low altitude also validate our record (Fig. 6 and Table 2).

On the orbital scale, we calculate the circulation regimes anomalies between the LGM and mid Holocene (MH) using the PMIP3 simulations (see Methods section). Fig. 5a and b show the averaged wind field at 700 hPa isobaric in summer during the MH and differential wind field at 700 hPa isobaric in summer between the LGM and MH, respectively. In the averaged state, the southerly wind is blown at 700 hPa, while in the differential field, the northerly wind is blown. This means that the EASM during the glacial is weaker than that in the interglacial, which is consistent with the reconstruction results of speleothem  $\delta^{18}\text{O}$  records from Dongge Cave and Hulu Cave (Yuan et al., 2004; Wang et al., 2001). Meanwhile, Fig. 5c and d show the averaged wind field at 200 hPa isobaric in ANN during the MH and differential wind field at 200 hPa isobaric in ANN between the LGM and MH, separately. The averaged wind fields during MH show that mid-latitude westerly jet stream mainly blows westerly wind and northerly wind (Fig. 5c). Meanwhile, the differential wind field between the LGM and MH is dominated by westerly wind and northerly wind at mid-latitudes (Fig. 5d). Thus, model results indicate that the westerly jet stream strengthened significantly during the LGM. In addition, the differences in the temperature, evaporation, precipitation and effective

moisture between the LGM and MH summers are obvious (Fig. 5e-h). Temperature, precipitation, and evaporation during the LGM are lower than those during the MH in the northern QTP. In order to clarify the moisture difference, the effective moisture represented by precipitation minus evaporation (P-E) was calculated (Fig. 5h). It can be seen that the effective moisture during the LGM in the northern QTP is slightly higher than that during the MH. Fig. 7 shows global climate changes between the 2090s, 2050s and 2010s according to median values of CMIP5 models (see Methods section). The summer temperature and precipitation are generally increasing from the 2010s to 2090s over the interaction zone between the EASM and the westerly jet stream in the mid-latitude regions, and the increasing amplitude is relatively large (Fig. 7a-d). The summer 500 hPa and 200 hPa wind fields all indicate a strengthening trend from the 2010s to 2090s (Fig. 7a-d), with the position of the westerly jet stream southward which is estimated by averaging the wind speed of the u-wind and v-wind from the 2010s to 2090s. (Fig. 7e-f).

## 5. Discussion

### 5.1. Climatic implication of stable isotope from surface sediments

Climate, i.e. precipitation and temperature, is the main factors controlling the formation and positioning of soil pedogenic carbonate (Eswaran et al., 2000; Zamanian et al., 2016). In paleoclimatology and paleoceanography,  $\delta^{18}\text{O}$  is a measure of stable isotopes  $^{18}\text{O}$ :  $^{16}\text{O}$ , but it is still controversial to explain the climatic implication of  $\delta^{18}\text{O}$ . In this paper, the more negative values of pedogenic carbonate are mostly distributed at high altitudes (Fig. 3b). We speculate that it may be due to the influence of multiple climatic factors in the vertical zone and the high-altitude westerly jet stream on a short time scale. According to the fractionation mechanism of oxygen isotopes, with increased temperature and evaporation,  $^{18}\text{O}$  of pedogenic carbonate is relatively enriched and the  $\delta^{18}\text{O}$  value is relatively high; while as temperature decreases and evaporation weakens,  $^{16}\text{O}$  of pedogenic carbonate is relatively enriched and the  $\delta^{18}\text{O}$  value is relatively low (Zhou et al., 2004). Vertical zones are obvious in the study area, so that evaporation in low-altitudes is much higher than that in high-altitudes. Therefore,  $^{16}\text{O}$  of surface sedimentary pedogenic carbonate in high-altitude is relatively enriched and the  $\delta^{18}\text{O}$  value is relatively low. In addition, the oxygen isotopic composition of modern soil carbonate can reflect the isotopic composition of local atmospheric water (Cerling, 1984; Quade et al., 2007). Data from the Global Network of Isotopes in Precipitation (GNIP) indicate that the precipitation in the area affected by westerly winds is negative (IAEA, 2006). According to the results of the modern wind field, it is obvious that the water vapor transported by the high-altitude westerly jet stream in the Qilian Mountains area has a greater contribution (Fig. 1c). The negative  $\delta^{18}\text{O}$  value at high altitude may also be a result of the westerly jet stream transportation. The analysis results related to meteorological elements show that pedogenic carbonate  $\delta^{18}\text{O}$  has a positive relationship with MAT and a negative correlation with MAP. Pedogenic carbonate  $\delta^{18}\text{O}$  values less than 290 mm have less fluctuations and are irrelevant to MAP (Fig. 3e), while pedogenic carbonate  $\delta^{18}\text{O}$  values greater than 290 mm are significantly inversely related to MAP. Modern climate research indicates that the annual average precipitation at the QL is 420 mm, therefore precipitation in the northern QTP has an inverse effect on carbonate  $\delta^{18}\text{O}$ . Taking into account the dual effects of temperature and precipitation on carbonate  $\delta^{18}\text{O}$ , we suggest that the carbonate  $\delta^{18}\text{O}$  changes in the northern QTP reflect the effective humidity.

Researchers have extensively used sedimentary  $\delta^{13}\text{C}_{\text{org}}$  data to track past C3/C4 relative abundance and climate change (Lin et al.,

1991; Galy et al., 2008). Changes of surface sedimentary  $\delta^{13}\text{C}$  are primarily influenced by climatic factors, i.e. temperature and precipitation (Rao et al., 2017). Temperature mainly affects enzyme activity, and precipitation mainly regulates the opening and closing of plant stomata through the absorption of  $\text{CO}_2$  during photosynthesis (Lipp et al., 1991; Zhao et al., 2017). Our results from surface sediments show that the  $\delta^{13}\text{C}_{\text{org}}$  values were mostly within the range of C3 plants. Many previous studies have shown that the carbon value of modern C3 plants is negatively correlated with precipitation (Zheng and Shangguan, 2007; Diefendorf et al., 2010; Kohn, 2010). Our results also support previous research, which demonstrate that the  $\delta^{13}\text{C}_{\text{org}}$  values of surface sediments under C3 vegetation (Fig. 3i-l) are more significantly negatively correlated with MAP than with MAT. The correlation is more significant when the precipitation is greater than 290 mm (Fig. 3l). This is mainly because the higher stomatal conductance of C3 plants increases the  $\text{CO}_2$  partial pressure between cells (Farquhar et al., 1989). Meanwhile, according to previous studies of organic geochemical proxies, the  $\delta^{13}\text{C}_{\text{org}}$  can reflect primary productivity and vegetation type in the arid regions (Krishnamurthy et al., 1986; Li et al., 2014). The carbon isotope in speleothem is largely controlled by local hydrology, soil and vegetation dynamics, and effective infiltration (Cheng et al., 2016a, 2016b). Therefore, the  $\delta^{13}\text{C}_{\text{org}}$  is an ideal indicator for the vegetation growth and moisture change in the northern QTP.

### 5.2. Paleoclimate change patterns in the northern QTP

In this study, the reconstructed climate change mode is relatively consistent with the NGRIP  $\delta^{18}\text{O}$ , which is different from simulated East Asian summer monsoon indices and isotopic distribution patterns along the monsoon vapor transport channel. As a widely used monsoon indicator, previous studies have used carbonate  $\delta^{18}\text{O}$  (‰) values from lakes and speleothems to represent the Holocene Asian summer monsoon variation (Wang, Y. et al., 2005; Zhang et al., 2011). However, the explanation of speleothem and lacustrine pedogenic carbonate  $\delta^{18}\text{O}$  has remained a great controversy (Cheng et al., 2009; Chen et al., 2015). Numerous studies suggested that the speleothem  $\delta^{18}\text{O}$  in southern China can be directly interpreted as reflecting the ASM intensity (Dykoski et al., 2005; Cheng et al., 2009; Liu et al., 2014). Due to complicated cave water cycle processes and water mixtures from multiple sources, however, whether speleothem  $\delta^{18}\text{O}$  can be directly used as an indicator of monsoon intensity is still uncertain (Cheng et al., 2009; Maher, 2008; Clemens et al., 2010).  $\delta^{18}\text{O}$  records in lacustrine carbonate sediments provide insights into past hydrological and climatic changes in East Asia (Yu et al., 2009). Compared with other sedimentary systems, surface sedimentary  $\delta^{18}\text{O}$  is directly affected by climate and environmental change (Ding and Zhang, 2005). Thus, in order to elucidate changes in atmospheric circulation patterns, it is necessary to develop credible indicators using surface sedimentary isotope in the northern QTP.

Modern climate in the study area is influenced by the interaction between the EASM and the westerly jet stream. Furthermore, our carbonate  $\delta^{18}\text{O}$  values greater than 290 mm from surface sediments are significantly inversely related to MAP. Modern climate research indicates that the annual average precipitation at the QL is 420 mm, therefore precipitation in the northern QTP has an inverse effect on carbonate  $\delta^{18}\text{O}$ . At the same time, the correlation analysis with MAT shows that  $\delta^{18}\text{O}$  values will also be affected by temperature in the northern QTP. As a result, the climate change mode in the mid-latitude mountain regions prevalently reflects effective moisture and the control of the westerly jet stream according to the reconstructed  $\delta^{18}\text{O}$  from the eolian sedimentary sequence. That is, since the LGM, when the westerly jet stream

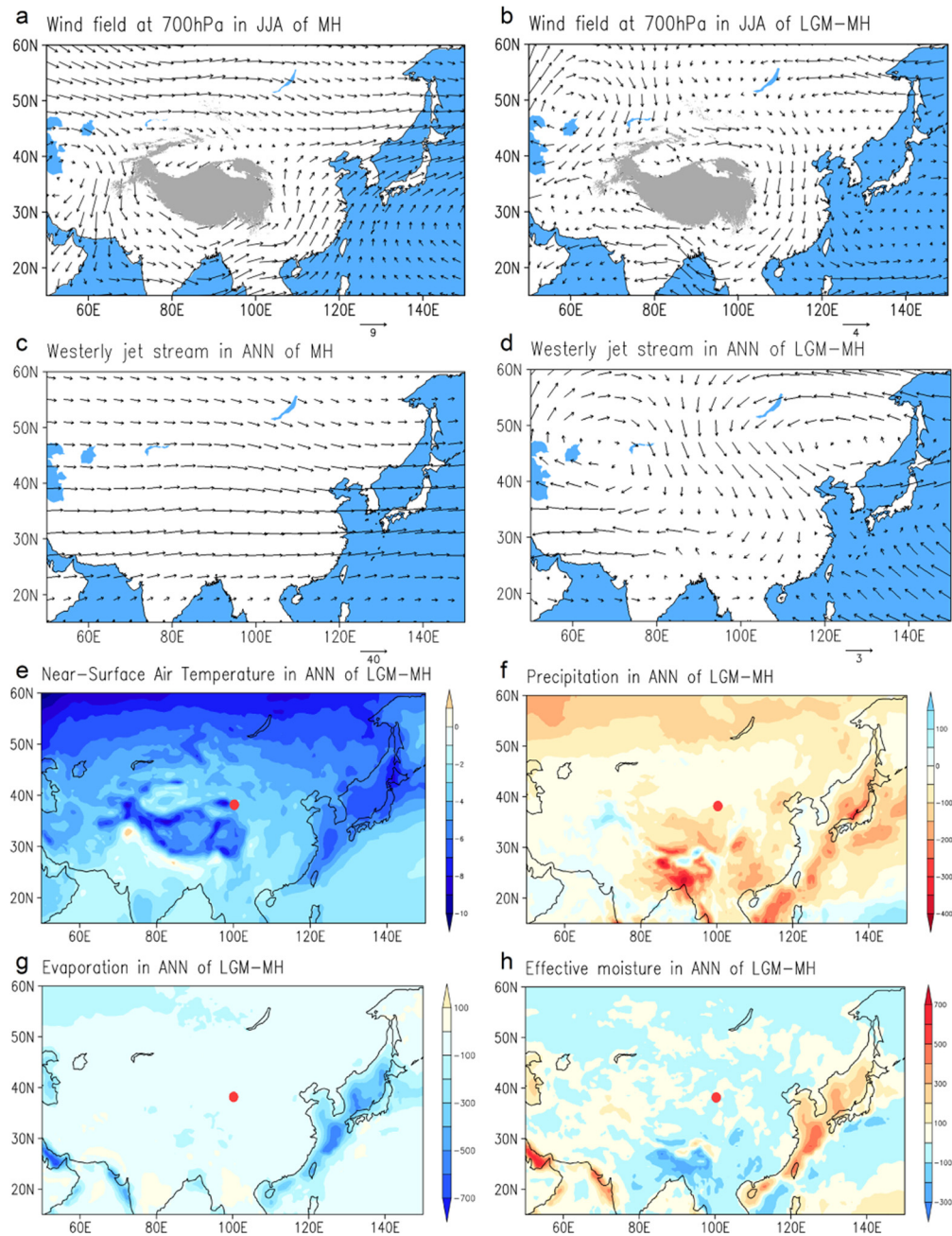


**Fig. 5.** The model simulation results from PMIP3. **a-b** Averaged wind field (m/s) at 700 hPa isobaric in summer (JJA) during the MH, and the differential wind field at 700 hPa isobaric in summer between the LGM and MH. **c-d** Averaged wind field (m/s) at 200 hPa isobaric in ANN (annual mean) during the MH, and the differential wind field at 200 hPa isobaric in ANN (annual mean) between the LGM and MH. **e-h** Difference of temperature ( $^{\circ}\text{C}$ ), evaporation (mm/mon), precipitation (mm/mon) and effective moisture (mm/mon) between the LGM and MH summers, respectively. The red dot represents the QL.

strengthens along with the increased zonal pressure gradient, the mountains become wetter.

$\delta^{13}\text{C}_{\text{org}}$  data from loess, lake, peat and marine records have been obtained to reconstruct the various time-scale paleovegetation and paleoclimate history (Hong et al., 2014; Ran and Feng, 2014; Rao et al., 2012; Wang et al., 2013; Zhang et al., 2018). On basis of the fact that temperature and precipitation mainly affect enzyme activity and precipitation regulates the opening and closing of plant stomata through the absorption of carbon dioxide in photosynthesis, temperature and precipitation are primarily responsible for change of  $\delta^{13}\text{C}_{\text{org}}$  values (Rao et al., 2017; Lipp et al., 1991; Wang and Feng, 2013; Zhao et al., 2017). Meanwhile, previous studies reveal that the  $\delta^{13}\text{C}_{\text{org}}$ , driven by effective moisture, can reflect primary productivity and vegetation type (Krish-

namurthy et al., 1986; Li et al., 2014). In addition, according to the interpretation of  $\delta^{13}\text{C}_{\text{org}}$  values from modern surface sediments, the  $\delta^{13}\text{C}_{\text{org}}$  is an ideal indicator of the vegetation growth state and the negative  $\delta^{13}\text{C}_{\text{org}}$  values always correspond to better vegetation growth state and moisture condition. During the last glaciation, the low  $\delta^{13}\text{C}_{\text{org}}$  value is consistent with the negative  $\delta^{18}\text{O}$  value showing the strong westerly water vapor transport in the northern QTP and its corresponding high effective moisture conditions.

Reconstructed feature of climate change during Holocene and LGM can also be found in simulation results. During the last glaciation, the PMIP3 simulation shows weaker EASM and stronger westerly jet stream, which made it difficult to transport monsoon vapor to the inland. In addition, studies have shown that the long shifts of coastlines in East and Southeast Asia related to sea level

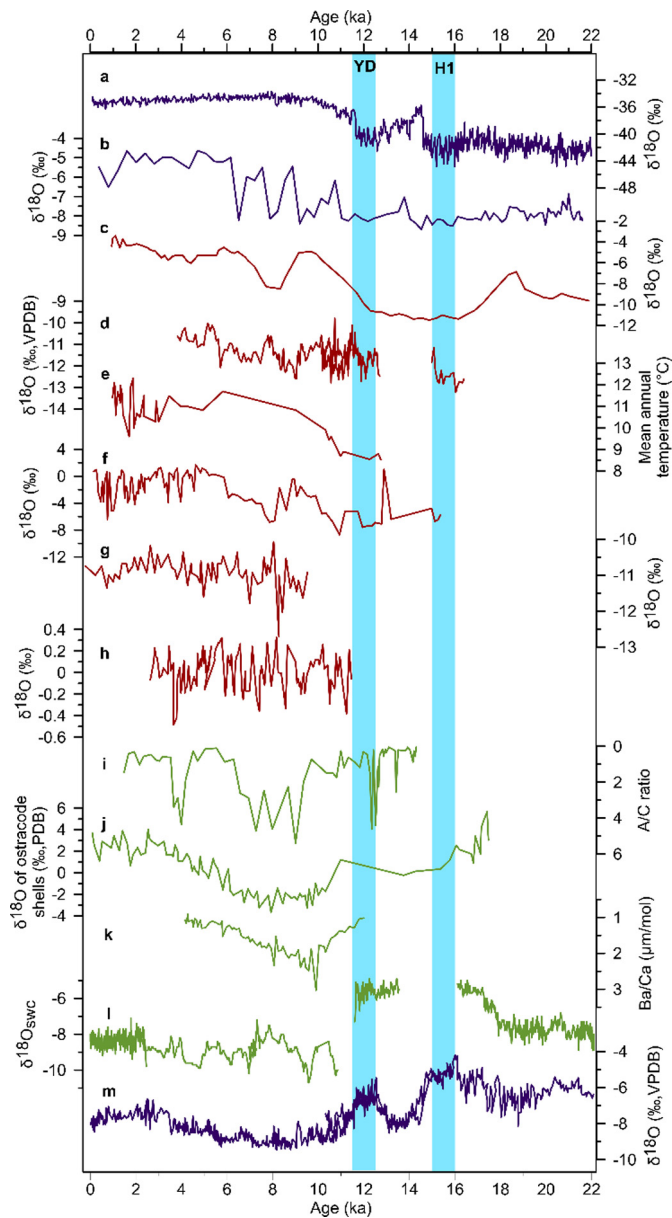


**Fig. 6.** Comparison of the Qilian eolian sedimentary record with other records in the mid-latitudes since the LGM. **a** NGRIP  $\delta^{18}\text{O}$  (Rasmussen et al., 2006). **b** The reconstructed carbonate  $\delta^{18}\text{O}$  from the QL (this study). **c-d**  $\delta^{18}\text{O}$  from Bear Lake and Lehman Caves, north America (Steponaitis et al., 2015; Dean et al., 2006). **e** Reconstructed mean annual temperature using Abo Arroyo  $\delta^{13}\text{C}$ , northern America (Hall and Penner, 2013). **f-g**  $\delta^{18}\text{O}$  from Hala Lake and Dundee Ice core (Yao and Thompson, 1992; Yan and Wünnemann, 2014). **h**  $\delta^{18}\text{O}$  from Grotte de Piste, northern Africa (Wassenburg et al., 2016). **i** Pollen A/C ratio from Yili Valley (Li et al., 2011). **j**  $\delta^{18}\text{O}$  of ostracode shells from Qinghai Lake (Liu et al., 2007). **k** Ba/Ca from the Levantine basin, northeastern Africa (Weldeab et al., 2014). **l**  $\delta^{18}\text{O}$  from Juxtlahuaca Cave, northern America (Lachniet et al., 2013). **m**  $\delta^{18}\text{O}$  from Dongge Cave and Hulu Cave (Yuan et al., 2004; Wang et al., 2001) (see Table 2).

changes may have played a crucial role in regulating the Asian inland summer monsoon on glacial-interglacial timescales (An et al., 2012). Increased transport distance makes water vapor more difficult to reach the northern QTP during the LGM. Therefore, we suggested that the monsoon rarely penetrate northwest to reach the northern QTP that is affected by modern monsoon water vapor in summer, while the high-altitude westerly jet stream affects the mountain climate. During the Holocene, both the amplitude and variability of the EASM increase obviously, especially in the early Holocene (Fig. 4b) (Dykoski et al., 2005; Yuan et al., 2004). However, since the LGM, the high-altitude carbonate  $\delta^{18}\text{O}$  values

in the northern QTP has a relatively stable trend, which is different from the EASM variation, but similar to the NGRIP  $\delta^{18}\text{O}$  record. It shows that carbonate  $\delta^{18}\text{O}$  values in mountainous areas are not controlled by monsoon vapor, the westerly jet stream transmits climate signals from Greenland to the global mid-latitude mountains. More importantly, the reconstructed climate variations in the global mid-latitude mountains exhibit this feature (Fig. 6c-h). Recently reported  $\delta^{18}\text{O}$  records of the mountains of Kesang Cave, Hoton-Nur, Dundee Ice core and Hala Lake in northeastern China, all show overall more positive trends since the LGM, and have been proposed as westerlies indicators (Cheng et al., 2016a,b; Rudaya et al., 2009; Yao and Thompson, 1992; Yan and Wünnemann, 2014). In the northern America and Africa, the reconstructed mean annual temperature, using Abo Arroyo  $\delta^{13}\text{C}$  and the  $\delta^{18}\text{O}$  proxies from Lehman Caves, Bear Lake and Grotte de Piste, is all similar to NGRIP  $\delta^{18}\text{O}$  evolution (Steponaitis et al., 2015; Dean et al., 2006; Hall and Penner, 2013; Wassenburg et al., 2016). Thus, we suggest that the westerly jet stream transmitted climate signals from Greenland to the global mid-latitude mountains, resulting in a unique climate mode (Porter and An, 1995). Conversely, the paleoclimate proxies from the low altitude regions of the mid-latitudes, such as West Nubian Paleolake and Levantine basin in northern Africa and Juxtlahuaca Cave in northern America, are consistent with the typical EASM records driven by the low latitude summer isolation (Fig. 6i-m). Noteworthy, because located in the monsoon water vapor transport channel, Qinghai Lake records indicate the influence of low latitude climate system obviously (Li et al., 2016).

With the modern global warming, the westerly jet stream strengthens and the Asian summer monsoon exhibits an obvious decrease tendency since 1980s (Li and Zeng, 2005; Yang and Zhang, 2007). This inference coincides with the simulation results of CMIP5 (Fig. 7). Over the next 100 yr, the westerlies at 500 hPa and 200 hPa will show an increasing trend (Fig. 7a-d), and the position of the westerly jet stream will also move southward (Fig. 7e-f). In this case, the mountain climate controlled by the westerly jet stream will be further humidified, which coincides with the trend of warming and humidification in the northwest of China (Shi, 2003; Wei and Wang, 2013). We suggest that understanding climate change in mid-latitude mountains and exploring the mechanism of interaction between the monsoon and the westerly jet stream can provide a useful scientific foundation for predictions.

## 6. Conclusions

We present a comprehensive analysis based on the combination of stable isotope reconstructions and ensemble simulations to explore the characteristics of the interaction between the EASM and the westerly jet stream. The carbonate  $\delta^{18}\text{O}$  indicates the change of effective humidity, while  $\delta^{13}\text{C}_{\text{org}}$  reflects the regional vegetation growth status. Since the LGM, change in humidity represented by  $\delta^{18}\text{O}$  in the eolian sedimentary sequence is consistent with that of the mountains in the global westerlies, and the vegetation conditions reflected by  $\delta^{13}\text{C}_{\text{org}}$  have less fluctuation. A comparison with other paleoclimate records around the world reveals that this feature is widespread in high-altitude regions at mid-latitudes, such as North American and African mountain regions. Under an acceleration of the warming trend in the future, the further intensification of the westerly jet stream will significantly increase humidity in the northern QTP.

## CRedit authorship contribution statement

**Yu Li:** Term, Conceptualization, Supervision, Project administration, Funding acquisition. **Simin Peng:** Methodology, Software, Data curation, Writing-original draft preparation. **Yu Li** and **Simin Peng:**

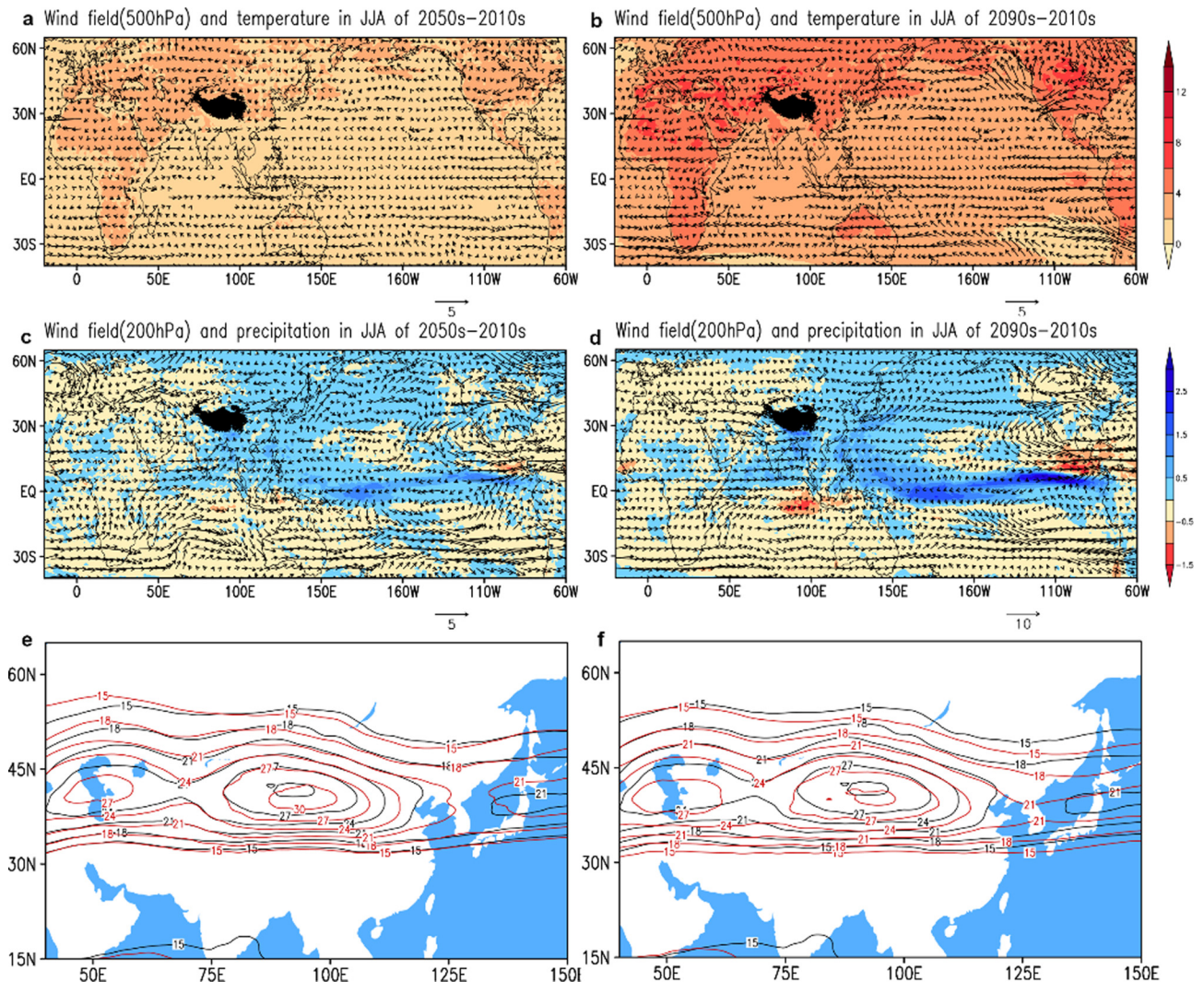


**Fig. 7.** The future predictions from CMIP5 models. **a–b** 500 hPa wind fields (m/s) and temperature ( $^{\circ}\text{C}$ ) in summer (JJA) from the 2010s to 2090s. **c–d** 200 hPa wind fields (m/s) and precipitation (mm/day) in summer (JJA) from the 2010s to 2090s. **e–f** Positions of the westerly jet streams in summer from the 2010s to 2090s.

Writing-review & editing, **Simin Peng, Hebin Liu, Xinzhong Zhang, Wangting Ye, Qin Han, Yuxin Zhang, Lingmei Xu, Yichan Li**: Visualization, Investigation.

#### Declaration of competing interest

The authors declare that they have no known competing financial interests or personal relationships that could have appeared to influence the work reported in this paper.

#### Acknowledgements

This work was supported by the National Natural Science Foundation of China (Grant No. 41822708), the Strategic Priority Research Program of Chinese Academy of Sciences (Grant No. XDA20100102), and the Second Tibetan Plateau Scientific Expedition and Research Program (STEP) (Grant No. 2019QZKK0202).

#### Appendix A. Supplementary material

Supplementary material related to this article can be found online at <https://doi.org/10.1016/j.epsl.2020.116529>.

#### References

- Abell, P.I., Hoelzmann, P., 2000. Holocene palaeoclimates in northwestern Sudan: stable isotope studies on molluscs. *Glob. Planet. Change* 26 (1–3), 1–12.
- Aguado, E., Burt, J.E., 2004. *Understanding Weather and Climate*, third ed. Prentice Hall, Upper Saddle River, New Jersey.
- Amundson, R.G., Chadwick, O.A., Sowers, J.M., Doner, H.E., 1988. Relationship between climate and vegetation and the stable carbon isotope chemistry of soils in the eastern Mojave Desert, Nevada. *Quat. Res.* 29, 245–254.
- An, Z., Colman, S.M., Zhou, W., Li, X., Brown, E.T., Jull, A.T., Cai, Y., Huang, Y., Lu, X., Chang, H., Song, Y., 2012. Interplay between the Westerlies and Asian monsoon recorded in Lake Qinghai sediments since 32 ka. *Sci. Rep.* 2, 619. <https://doi.org/10.1038/srep00619>.
- Barry, R.G., Chorley, R.J., Yokoi, N.J., 2004. *Atmosphere, Weather, and Climate*, eighth ed. Routledge, London.
- Berger, A.L., 1978. Long-term variations of caloric insolation resulting from the Earth's orbital elements. *Quat. Res.* 9, 139–167.
- Brown, P.T., Caldeira, K., 2017. Greater future global warming inferred from Earth's recent energy budget. *Nature* 552, 45–50.
- Cerling, T.E., 1984. The stable isotopic composition of modern soil carbonate and its relationship to climate. *Earth Planet. Sci. Lett.* 71, 229–240.
- Chen, F., Chen, J., Huang, W., Chen, S., Huang, X., Jin, L., Jia, J., Zhang, X., An, C., Zhang, J., Zhao, Y., 2019. Westerlies Asia and monsoonal Asia: spatiotemporal differences in climate change and possible mechanisms on decadal to sub-orbital timescales. *Earth-Sci. Rev.* 192, 337–354.
- Chen, F., Xu, Q., Chen, J., Birks, H.J.B., Liu, J., Zhang, S., Jin, L., An, C., Telford, R.J., Cao, X., Wang, Z., 2015. East Asian summer monsoon precipitation variability since the last deglaciation. *Sci. Rep. UK* 5, 11186.
- Chen, F., Yu, Z., Yang, M., Ito, E., Wang, S., Madsen, D.B., Huang, X., Zhao, Y., Sato, T., Birks, H.J.B., Boomer, I., 2008. Holocene moisture evolution in arid central Asia

- and its out-of-phase relationship with Asian monsoon history. *Quat. Sci. Rev.* 27, 351–364.
- Cheng, H., Edwards, R.L., Broecker, W.S., Denton, G.H., Kong, X., Wang, Y., Zhang, R., Wang, X., 2009. Ice age terminations. *Science* 326, 248–252.
- Cheng, H., Edwards, R.L., Sinha, A., Spötl, C., Yi, L., Chen, S., Kelly, M., Kathayat, G., Wang, X., Li, X., Kong, X., 2016a. The Asian monsoon over the past 640000 years and ice age terminations. *Nature* 534, 640–646.
- Cheng, H., Spötl, C., Breitenbach, S.F., Sinha, A., Wassenburg, J.A., Jochum, K.P., Scholz, D., Li, X., Yi, L., Peng, Y., Lv, Y., 2016b. Climate variations of central Asia on orbital to millennial timescales. *Sci. Rep.* 5, 36975. <https://doi.org/10.1038/srep36975>.
- Chiang, J.C., Fung, I.Y., Wu, C.H., Cai, Y., Edman, J.P., Liu, Y., Day, J.A., Bhattacharya, T., Mondal, Y., Labrousse, C.A., 2015. Role of seasonal transitions and westerly jets in East Asian paleoclimate. *Quat. Sci. Rev.* 108, 111–129.
- Clemens, S.C., Prell, W.L., Sun, Y., 2010. Orbital-scale timing and mechanisms driving Late Pleistocene Indo-Asian summer monsoons: reinterpreting cave speleothem  $\delta^{18}\text{O}$ . *Paleoceanography* 25 (4).
- COHMAP Members, 1988. Climatic changes of the last 18,000 years: observations and model simulations. *Science* 241, 1043–1052.
- Davis, M.E., Thompson, L.G., Yao, T., Wang, N., 2005. Forcing of the Asian monsoon on the Tibetan Plateau: evidence from high-resolution ice core and tropical coral records. *J. Geophys. Res., Atmos.* 110 (D4).
- Dean, W., Rosenbaum, J., Skipp, G., Colman, S., Forester, R., Liu, A., Simmons, K., Bischoff, J., 2006. Unusual Holocene and late Pleistocene carbonate sedimentation in bear lake, Utah and Idaho, USA. *Sediment. Geol.* 185, 93–112. <https://doi.org/10.1016/j.sedgeo.2005.11.016>.
- Deines, P., 1980. The isotopic composition if reduced organic carbon. In: Fritz, P., Fontes, J.C. (Eds.), *Handbook of Environmental Isotope Geochemistry The Terrestrial Environment*. Elsevier, Dordrecht, pp. 339–345.
- Diefendorf, A.F., Mueller, K.E., Wing, S.L., Koch, P.L., Freeman, K.H., 2010. Global patterns in leaf  $^{13}\text{C}$  discrimination and implications for studies of past and future climate. *Proc. Natl. Acad. Sci. USA* 107, 5738–5743.
- Ding, H., Zhang, J., 2005. Geochemical properties and evolution of groundwater beneath the Hexi Corridor, Gansu Province. *Arid Zone Res.* 22, 24–28 (in Chinese).
- Ding, Z.L., Rutter, N.W., Liu, T.S., Sun, J.M., Ren, J.Z., Rokosh, D., Xiong, S.F., 1998. Correlation of Dansgaard Oeschger cycles between Greenland ice and Chinese loess. *Paleoclimates* 4, 281–291.
- Dykoski, C.A., Edwards, R.L., Cheng, H., Yuan, D., Cai, Y., Zhang, M., Lin, Y., Qing, J., An, Z., Revenaugh, J., 2005. A high-resolution, absolute-dated Holocene and deglacial Asian monsoon record from Dongge Cave, China. *Earth Planet. Sci. Lett.* 233, 71–86.
- Eswaran, H., Reich, P.F., Kimble, J.M., Beinroth, F.H., Padmanabhan, E., Moncharoen, P., 2000. Global carbon stocks. In: Lal, R., Kimble, J.M., Eswaran, H., Stewart, B.A. (Eds.), *Global Climate Change and Pedogenic Carbonates*. CRC Press, Boca Raton, Fla, pp. 15–25.
- Farquhar, G.D., Ehleringer, J.R., Hubick, K.T., 1989. Carbon isotope discrimination and photosynthesis. *Annu. Rev. Plant Physiol. Plant Mol. Biol.* 40, 503–537.
- Galy, V., François, L., France-Lanord, C., Faure, P., Kudrass, H., Palhol, F., Singh, S.K., 2008. C4 plants decline in the Himalayan basin since the Last Glacial Maximum. *Quat. Sci. Rev.* 27, 1396–1409.
- Hall, S.A., Penner, W.L., 2013. Stable carbon isotopes, C3–C4 vegetation, and 12,800 years of climate change in central New Mexico, USA. *Palaeogeogr. Palaeoclimatol. Palaeoecol.* 369, 272–281. <https://doi.org/10.1016/j.palaeo.2012.10.034>.
- Harris, I., Jones, P.D., Osborn, T.J., Lister, D.H., 2013. Updated high-resolution grids of monthly climatic observations—the CRU TS3.10 dataset. *Int. J. Climatol.* 34, 623–642.
- He, F., 2011. *Simulating Transient Climate Evolution of the Last Deglaciation with CCSM3*. Department of Atmospheric and Oceanic Sciences, University of Wisconsin, Madison, p. 171.
- He, Y., Zhao, C., Liu, Z., Wang, H., Liu, W., Yu, Z., Zhao, Y., Ito, E., 2016. Holocene climate controls on water isotopic variations on the northeastern Tibetan Plateau. *Chem. Geol.* 440, 239–247.
- Herzschuh, U., Cao, X., Laepple, T., Dallengier, A., Telford, R.J., Ni, J., Chen, F., Kong, Z., Liu, G., Liu, K.B., Liu, X., 2019. Position and orientation of the westerly jet determined Holocene rainfall patterns in China. *Nat. Commun.* 10, 2376. <https://doi.org/10.1038/s41467-019-09866-8>.
- Hong, B., Gasse, F., Uchida, M., Hong, Y.T., Leng, X.T., Shibata, Y., An, N., Zhu, Y.X., Wang, Y., 2014. Increasing summer rainfall in arid eastern-Central Asia over the past 8500 years. *Sci. Rep.* 4, 5279.
- Huang, C.M., Wang, C.H., Ai, N.S., 2003. Implication and application of stable carbon and oxygen isotopes of pedogenic carbonates in soils. *Adv. Earth Sci.* 18, 132–138 (in Chinese).
- IAEA/WMO, A.A.A., 2006. *Global Network of Isotopes in Precipitation*. The GNIP database.
- Joussaume, S., Taylor, K.E., Braconnot, P.J.F.B., Mitchell, J.F.B., Kutzbach, J.E., Harrison, S.P., Prentice, I.C., Broccoli, A.J., Abe-Ouchi, A., Bartlein, P.J., Bonfils, C., 1999. Monsoon changes for 6000 years ago: results of 18 simulations from the paleoclimate modeling intercomparison project (PMIP). *Geophys. Res. Lett.* 26, 859–862.
- Kalnay, E., Kanamitsu, M., Kistler, R., Collins, W., Deaven, D., Gandin, L., Iredell, M., Saha, S., White, G., Woollen, J., Zhu, Y., 1996. The NCEP/NCAR 40-year reanalysis project. *Bull. Am. Meteorol. Soc.* 77, 437–472. [https://doi.org/10.1175/1520-0477\(1996\)077<0437:TNYRP>2.0.CO;2](https://doi.org/10.1175/1520-0477(1996)077<0437:TNYRP>2.0.CO;2).
- Kohn, M.J., 2010. Carbon isotope compositions of terrestrial C3 plants as indicators of (paleo) ecology and (paleo)climate. *Proc. Natl. Acad. Sci. USA* 107, 19691–19695.
- Kong, W., Swenson, L.M., Chiang, J.C.H., 2017. Seasonal transitions and the Westerly Jet in the Holocene East Asian Summer Monsoon. *J. Climate* 30 (9), 3343–3365. <https://doi.org/10.1175/jcli-d-16-0087.1>.
- Krishnamurthy, R.V., Bhattacharya, S.K., Kusumgar, S., 1986. Palaeoclimatic changes deduced from  $^{13}\text{C}/^{12}\text{C}$  and C/N ratios of Karewa lake sediments, India. *Nature* 323 (6084), 150.
- Kutzbach, J., Gutter, P., Behling, P.C.J., Selin, R., 1993. Simulated climatic changes: results of the COHMAP climate-model experiments. In: Wright, H.E., Kutzbach, J.E., Webb III, T., Ruddiman, W.F., Street-Perrott, F.A., Bartlein, P.J. (Eds.), *Global Climates since the Last Glacial Maximum*. University of Minnesota Press, London, pp. 24–93.
- Lachniet, M.S., Asmerom, Y., Bernal, J.P., Polyak, V.J., Vazquez-Selem, L., 2013. Orbital pacing and ocean circulation-induced collapses of the Mesoamerican monsoon over the past 22,000 y. *Proc. Natl. Acad. Sci.* 110 (23), 9255–9260. <https://doi.org/10.1073/pnas.1222804110>.
- Li, J.P., Zeng, Q.C., 2005. A new monsoon index, its interannual variability and relation with monsoon precipitation. *Clim. Environ. Res.* 3, 73–87 (in Chinese).
- Li, X., Zhao, K., Dodson, J., Zhou, X., 2011. Moisture dynamics in central Asia for the last 15 kyr: new evidence from Yili Valley, Xinjiang, NW China. *Quat. Sci. Rev.* 30 (23–24), 3457–3466. <https://doi.org/10.1016/j.quascirev.2011.09.010>.
- Li, Y., Chen, H., Li, Z., Zhou, X., Zhang, C., 2012. Tracking millennial-scale climate change by analysis of the modern summer precipitation in the marginal regions of the Asian monsoon. *J. Asian Earth Sci.* 58, 78–87.
- Li, Y., Zhang, C., Wang, Y., 2016. The verification of millennial-scale monsoon water vapor transport channel in northwest China. *J. Hydrol.* 536, 273–283.
- Li, Y., Zhou, X., Zhang, C., Li, Z., Wang, Y., Wang, N., 2014. Relationship between pollen assemblages and organic geochemical proxies and the response to climate change in the Zhuye Lake sediments. *Sci. Cold Arid Reg.* 6 (1), 37–43.
- Lin, B.H., Liu, R.M., An, Z.S., 1991. Preliminary research on stable isotopic composition of Chinese Loess. In: Liu, T.S. (Ed.), *Loess, Environment and Global Change*. Science Press, Beijing, pp. 124–131.
- Lipp, J., Trimborn, P., Fritz, P., Moser, H., Becker, B., Frenzel, B., 1991. Stable isotopes in tree ring cellulose and climatic change. *Tellus B* 43 (3), 322–330.
- Liu, X.Q., Shen, J., Wang, S.M., Wang, Y.B., Liu, W.G., 2007. Southwest monsoon changes indicated by oxygen isotope of ostracode shells from sediments in qinghai lake since the late glacial. *Chin. Sci. Bull.* 4, 109–114.
- Liu, Z., Otto-Bliesner, B.L., He, F., Brady, E.C., Tomas, R., Clark, P.U., Carlson, A.E., Lynch-Stieglitz, J., Curry, W., Brook, E., Erickson, D., 2009. Transient simulation of last deglaciation with a new mechanism for Bölling-Allerød warming. *Science* 325, 310–314.
- Liu, Z., Wen, X., Brady, E.C., Otto-Bliesner, B., Yu, G., Lu, H., Cheng, H., Wang, Y., Zheng, W., Ding, Y., Edwards, R.L., 2014. Chinese cave records and the East Asia summer monsoon. *Quat. Sci. Rev.* 83, 115–128. <https://doi.org/10.1016/j.quascirev.2013.10.021>.
- Maher, B.A., 2008. Holocene variability of the East Asian summer monsoon from Chinese cave records: a re-assessment. *Holocene* 18, 861–866.
- Meyers, P.A., Lallier-Vergès, E., 1999. Lacustrine sedimentary organic matter records of Late Quaternary paleoclimates. *J. Paleolimnol.* 21 (3), 345–372.
- Moss, R., Edmonds, J., Hibbard, K., 2010. The next generation of scenarios for climate change research and assessment. *Nature* 463, 747–756.
- Nagashima, K., Tada, R., Tani, A., Sun, Y., Isozaki, Y., Toyoda, S., Hasegawa, H., 2011. Millennial-scale oscillations of the westerly jet path during the last glacial period. *J. Asian Earth Sci.* 40, 1214–1220.
- O’Leary, M.H., 1988. Carbon isotope in photosynthesis. *Bioscience* 38, 328–336.
- Overland, J.E., Dethloff, K., Francis, J.A., Hall, R.J., Hanna, E., Kim, S.J., Screen, J.A., Shepherd, T.G., Vihma, T., 2006. Nonlinear response of mid-latitude weather to the changing Arctic. *Nat. Clim. Change* 6, 992–999.
- Porter, S.C., An, Z.S., 1995. Correlation between climate events in the North Atlantic and China during the last glaciation. *Nature* 375, 305–308.
- Quade, J., Garzzone, C., Eiler, J., 2007. Paleoelevation reconstruction using pedogenic carbonates. *Rev. Mineral. Geochem.* 66, 53–87.
- Ramsey, C.B., Lee, S., 2013. Recent and planned developments of the program OxCal. *Radiocarbon* 55 (2), 720–730.
- Ran, M., Feng, Z.D., 2014. Variation in carbon isotopic composition over the past ca. 46,000 yr in the loess-Paleosol sequence in central Kazakhstan and paleoclimatic significance. *Org. Geochem.* 73, 47–55.
- Rao, Z., Guo, W., Cao, J., Shi, F., Jiang, H., Li, C., 2017. Relationship between the stable carbon isotopic composition of modern plants and surface soils and climate: a global review. *Earth-Sci. Rev.* 165, 110–119.
- Rao, Z., Wu, D., Shi, F., Guo, H., Cao, J., Chen, F., 2019. Reconciling the ‘westerlies’ and ‘monsoon’ models: a new hypothesis for the Holocene moisture evolution of the Xinjiang region, NW China. *Earth-Sci. Rev.* 191, 263–272.
- Rao, Z.G., Chen, F.H., Zhang, X., Xu, Y.B., Xue, Q., Zhang, P.Y., 2012. Spatial and temporal variations of C3/C4 relative abundance in global terrestrial ecosystem

- since the Last Glacial and its possible driving mechanisms. *Chin. Sci. Bull.* 57, 4024–4035.
- Rasmussen, S.O., Andersen, K.K., Svensson, A.M., Steffensen, J.P., Vinther, B.M., Clausen, H.B., Siggaard-Andersen, M.L., Johnsen, S.J., Larsen, L.B., Dahl-Jensen, D., Bigler, M., 2006. A new Greenland ice core chronology for the last glacial termination. *J. Geophys. Res.* 111, D06102. <https://doi.org/10.1029/2005JD006079>.
- Reimer, P.J., Bard, E., Bayliss, A., Beck, J.W., Blackwell, P.G., Ramsey, C.B., Buck, C.E., Cheng, H., Edwards, R.L., Friedrich, M., Grootes, P.M., 2013. IntCal13 and Marine13 radiocarbon age calibration curves 0–50,000 years cal BP. *Radiocarbon* 55 (4), 1869–1887.
- Roberts, N., Jones, M.D., Benkaddour, A., Eastwood, W.J., Filippi, M.L., Frogley, M.R., Lamb, H.F., Leng, M.J., Reed, J.M., Stein, M., Stevens, L., 2008. Stable isotope records of Late Quaternary climate and hydrology from Mediterranean lakes: the ISOMED synthesis. *Quat. Sci. Rev.* 27 (25–26), 2426–2441.
- Rudaya, N., Tarasov, P., Dorofeyuk, N., Solovieva, N., Kalugin, I., Andreev, A., Daryin, A., Diekmann, B., Riedel, F., Tserendash, N., Wagner, M., 2009. Holocene environments and climate in the Mongolian Altai reconstructed from the Hotoon-Nur pollen and diatom records: a step towards better understanding climate dynamics in Central Asia. *Quat. Sci. Rev.* 28 (5–6), 540–554. <https://doi.org/10.1016/j.quascirev.2008.10.013>.
- Sampe, T., Xie, S.-P., 2010. Large-scale dynamics of the Meiyu-Baiu rainband: environmental forcing by the Westerly Jet. *J. Climate* 23, 113–134.
- Schiemann, R., Lüthi, D., Schär, C., 2009. Seasonality and interannual variability of the westerly jet in the Tibetan Plateau region. *J. Climate* 22, 2940–2957.
- Shi, Y.F., 2003. Discussion on the present climate change from warm-dry to warm-wet in northwest China. *Quat. Sci.* 23 (2), 152–164.
- Steponaitis, E., Andrews, A., McGee, D., Quade, J., Hsieh, Y.T., Broecker, W.S., Shuman, B.N., Burns, S.J., Cheng, H., 2015. Mid-Holocene drying of the U.S. Great Basin recorded in Nevada speleothems. *Quat. Sci. Rev.* 127, 174–185. <https://doi.org/10.1016/j.quascirev.2015.04.011>.
- Stuiver, M., Grootes, P.M., Braziunas, T.F., 1995. The GISP2  $\delta^{18}\text{O}$  climate record of the past 16,500 years and the role of the sun, ocean, and volcanoes. *Quat. Res.* 44 (3), 341–354.
- Sun, Y., Kutzbach, J., An, Z., Clemens, S., Liu, Z., Liu, W., Liu, X., Shi, Z., Zheng, W., Liang, L., Yan, Y., Li, Y., 2015. Astronomical and glacial forcing of East Asian summer monsoon variability. *Quat. Sci. Rev.* 115, 132–142.
- Taylor, K.E., Stouffer, R.J., Meehl, G.A., 2012. An overview of CMIP5 and the experiment design. *Bull. Am. Meteorol. Soc.* 934, 485–498.
- Wang, G.A., Li, J., Liu, X., Li, X., 2013. Variations in carbon isotope ratios of plants across a temperature gradient along the 400 mm isohaline of mean annual precipitation in north China and their relevance to paleovegetation reconstruction. *Quat. Sci. Rev.* 63, 83–90.
- Wang, K., Jiang, H., Zhao, H., 2005. Atmospheric water vapor transport from westerly and monsoon over the northwest China. *Adv. Water Sci.* 16, 432–438 (in Chinese).
- Wang, N., Liu, W.G., 2010. Carbonate content and oxygen and carbon isotope composition of different grain size samples from the surface soil of arid land in northwest China. *Arid Land Geogr.* 2, 10–15 (in Chinese).
- Wang, S., Zuo, H., Zhao, S., Zhang, J., Lu, S., 2017. How East Asian westerly jet's meridional position affects the summer rainfall in Yangtze-Huaihe River Valley? *Clim. Dyn.* 25.
- Wang, W., Feng, Z.D., 2013. Holocene moisture evolution across the Mongolian Plateau and the surrounding areas, a synthesis of climatic records. *Earth-Sci. Res. Rev.* 22, 38–57.
- Wang, Y., Cheng, H., Edwards, R.L., He, Y., Kong, X., An, Z., Wu, J., Kelly, M.J., Dykoski, C.A., Li, X., 2005. The Holocene Asian monsoon: links to solar changes and North Atlantic climate. *Science* 308 (5723), 854–857.
- Wang, Y.J., Cheng, H., Edwards, R.L., An, Z.S., Wu, J.Y., Shen, C.C., Dorale, J.A., 2001. A high-resolution absolute-dated late Pleistocene monsoon record from hulu cave, China. *Science* 294 (5550), 2345–2348. <https://doi.org/10.1126/science.1064618>.
- Wang, Y.Q., Zhang, X.Y., Arimoto, R., Cao, J.J., Shen, Z.X., 2005. Characteristics of carbonate content and carbon and oxygen isotopic composition of northern China soil and dust aerosol and its application to tracing dust sources. *Atmos. Environ.* 39, 2631–2642.
- Wassenburg, J.A., Dietrich, S., Fietzke, J., Fohlmeister, J., Jochum, K.P., Scholz, D., Richter, D.K., Sabaoui, A., Spötl, C., Lohmann, G., Andreae, M.O., 2016. Reorganization of the North Atlantic oscillation during early Holocene deglaciation. *Nat. Geosci.* 9 (8), 602–605. <https://doi.org/10.1038/ngeo2767>.
- Wei, K., Gasse, F., 1999. Oxygen isotopes in lacustrine carbonates of West China revisited: implications for post glacial changes in summer monsoon circulation. *Quat. Sci. Rev.* 18 (12), 1315–1334.
- Wei, K., Wang, L., 2013. Reexamination of the aridity conditions in arid northwestern China for the last decade. *J. Climate* 26 (23), 9594–9602.
- Weldeab, S., Menke, V., Schmiedl, G., 2014. The pace of East African monsoon evolution during the Holocene. *Geophys. Res. Lett.* 41 (5), 1724–1732. <https://doi.org/10.1002/2014gl059361>.
- Wu, L., Li, C., Yang, C., 2008. Global teleconnections in response to a shutdown of the Atlantic meridional overturning circulation. *J. Climate* 21, 3002–3019.
- Yan, D., Wünnemann, B., 2014. Late Quaternary water depth changes in Hala Lake, northeastern Tibetan Plateau, derived from ostracod assemblages and sediment properties in multiple sediment records. *Quat. Sci. Rev.* 95, 95–114. <https://doi.org/10.1016/j.quascirev.2014.04.030>.
- Yancheva, G., Nowaczyk, N.R., Mingram, J., Dulski, P., Schettler, G., Negendank, J.F., Liu, J., Sigman, D.M., Peterson, L.C., Haug, G.H., 2007. Influence of the intertropical convergence zone on the East Asian monsoon. *Nature* 445, 74–77.
- Yang, L.M., Zhang, Q.Y., 2007. Anomalous perturbation kinetic energy of Rossby Wave along East Asian Westerly Jet and its association with summer rainfall in China. *Chin. J. Atmos. Sci.* 4, 28–37 (in Chinese).
- Yao, T., Masson-Delmotte, V., Gao, J., Yu, W., Yang, X., Risi, C., Sturm, C., Werner, M., Zhao, H., He, Y., Ren, W., 2013. A review of climatic controls on  $\delta^{18}\text{O}$  in precipitation over the Tibetan Plateau: observations and simulations. *Rev. Geos.* 51 (4), 525–548.
- Yao, T., Thompson, L.G., 1992. Dunde ice core record and past 5 ka temperature change. *Sci. China*, M(10)x (in Chinese).
- Yeager, S., Shields, C., Large, W., Hack, J., 2003. The low-resolution CCSM3. *J. Climate* 19, 2545–2566.
- Yu, S., Ricketts, R.D., Colman, S.M., 2009. Determining the spatial and temporal patterns of climate changes in China's western interior during the last 15 ka from lacustrine oxygen isotope records. *J. Quat. Sci.* 24, 237–247.
- Yuan, D., Cheng, H., Edwards, R.L., Dykoski, C.A., Kelly, M.J., Zhang, M., Qing, J., Lin, Y., Wang, Y., Wu, J., Dorale, J.A., 2004. Timing, duration, and transitions of the last interglacial Asian monsoon. *Science* 304 (5670), 575–578.
- Zamanian, K., Pustovoytov, K., Kuzyakov, Y., 2016. Pedogenic carbonates: forms and formation processes. *Earth-Sci. Rev.* 157, 1–17.
- Zhang, D., Yang, Y., Ran, M., 2019. Variations of surface soil  $\delta^{13}\text{C}_{\text{org}}$  in the different climatic regions of China and paleoclimatic implication. *Quat. Int.* 536, 92–102.
- Zhang, D.L., Feng, Z.D., Lan, B., Yang, Y.P., Ran, M., Mu, G.J., 2018. Peat  $\delta^{13}\text{C}$  cellulose-recorded wetting trend during the past 8000 years in the southern Altai Mountains within China and the possible reasons. *J. Asian Earth Sci.* 156, 174–179.
- Zhang, H.C., Zhang, L.Y., Zhang, W.X., 1990. Studies on carbon and oxygen isotopic geochemical characteristics and loess sedimentation of Jiuzhoutai loess profile, Lanzhou. *J. Lanzhou Univ.* 26, 117–126 (in Chinese).
- Zhang, J.C., Lin, Z.G., 1992. *Climate of China*. Wiley, New York.
- Zhang, J., Chen, F., Holmes, J.A., Li, H., Guo, X., Wang, J., Li, S., Lü, Y., Zhao, Y., Qiang, M., 2011. Holocene monsoon climate documented by oxygen and carbon isotopes from lake sediments and peat bogs in China: a review and synthesis. *Quat. Sci. Rev.* 30, 1973–1987.
- Zhao, S.Q., 1983. A new scheme for comprehensive physical regionalization in China. *Acta Geogr. Sin.* 38, 1–10 (in Chinese).
- Zhao, Y., Wu, F.L., Fang, X.M., Yang, Y.B., 2017. Altitudinal variations in the bulk organic carbon isotopic composition of topsoil in the Qilian Mountains area, NE Tibetan Plateau, and its environmental significance. *Quat. Int.* 454, 45–55.
- Zhou, D.J., Ma, H.Z., Gao, D.L., Ma, W.D., Tan, H.B., Xu, L.M., 2004. Geochemical characteristics and climatic environmental significance of Holocene loess on South Qinghai Lake shore. *J. Desert Res.* 24 (2), 144–148 (in Chinese).
- Zheng, S.X., Shangguan, Z.P., 2007. Spatial patterns of foliar stable carbon isotope compositions of C3 plant species in the Loess Plateau of China. *Ecol. Res.* 22, 342–353.